Untargeted proteomics identifies plant substrates of the bacterial-derived ADP-ribosyltransferase AvrRpm1

Simranjit Kaur[a], Thomas Colby[b], Domenika Thieme[a], Carsten Proksch[a], Susanne Matschi[a], Ivan Matić[b], Lennart Wirthmueller[a,c]

[a]Leibniz Institute of Plant Biochemistry, Department Biochemistry of Plant Interactions, Weinberg 3, 06120 Halle (Saale), Germany

[b]Research Group of Proteomics and ADP-ribosylation Signaling, Max Planck Institute for Biology of Ageing, 50931 Cologne, Germany

[c]Corresponding author: lennart.wirthmueller@ipb-halle.de

Abstract

One class of enzymes that plant pathogens employ to manipulate innate immunity and physiology of the infected cells are host-targeted ADP-ribosyltransferases. The bacterial pathogen *Pseudomonas syringae* uses its type III secretion system to inject several effector proteins with ADP-ribosyltransferase activity into plant cells. One of them, AvrRpm1, ADP-ribosylates the plasma membrane-associated RPM1-INTERACTING PROTEIN 4 (RIN4) in *Glycine max* and *Arabidopsis thaliana* to attenuate targeted secretion of defense-promoting compounds. Substrate identification of host-targeted ADP-ribosyltransferases is complicated by the biochemical lability of the protein modification during plant protein extraction and in several cases required prior knowledge on plant immune signaling pathways that are impaired by the ADP-ribosylating type III effector. Using the AvrRpm1-RIN4 pair as a proof-of-concept, we present an untargeted proteomics workflow for enrichment and detection of ADP-ribosylated proteins and peptides from plant cell extracts that in several cases provides site-resolution for the modification.

Introduction

The ability to limit activation of plant innate immunity is a pre-requisite for successful infection by microbial pathogens (Wang et al., 2022). The Gram-negative bacterial pathogen *Pseudomonas syringae* pv. *tomato* (*Pst*) injects 29 type III effectors (T3Es) into the host cell cytoplasm where they cooperatively manipulate host physiology and suppress plant immune responses triggered by activation of cell surface localized pattern recognition receptors (pattern-triggered immunity, PTI) (Xin et al., 2016; Cunnac et al., 2011). Recognition of microbe-associated molecular patterns by pattern recognition receptors activates PTI that is effective against attempted invasion by non-adapted pathogens. In contrast, well-adapted pathogens effectively subvert PTI by translocating effectors into plant cells (Wang et al., 2022). Immunity against such adapted pathogens in plants is conferred by a second class of intracellular immune receptors, nucleotide-binding domain leucine-rich repeat receptors (NLRs), in a cultivar-specific manner (Saur et al., 2021). This form of NLR-

mediated resistance to specific pathogen isolates is known as effector-triggered immunity (ETI) (Saur et al., 2021). NLRs detect pathogen effectors either directly or they form protein complexes with virulence targets of effectors and sense effector-mediated manipulation of the 'guarded' plant proteins (Wang et al., 2019; Martin et al., 2020). Therefore, the outcome of an infection attempt by an adapted pathogen depends on both, the set of effectors delivered by the pathogen and the NLR repertoire of the plant. In the absence of NLR-mediated recognition effectors promote pathogen virulence (Wang et al., 2022). In contrast, in interactions where at least one effector is recognized by an NLR, the plant rapidly activates ETI that limits further pathogen spread and often involves localized programmed cell death at the site of infection (Saur et al., 2021).

Many bacterial T3Es are host-targeted enzymes that manipulate plant proteins by post-translational modifications to perturb activation of plant immunity (Wang et al., 2022). Among the T3Es that *Pst* strain DC3000 injects into plant cells are several ADP-ribosyltransferases that modify host proteins by transfer of the ADP-ribose (ADPr) moiety from nicotinamide adenine dinucleotide (NAD^+) onto amino acid side chains (Fu et al., 2007; Wang et al., 2010; Aung et al., 2020; Rack et al., 2020). The T3E HopF2 ADP-ribosylates Arabidopsis MITOGEN-ACTIVATED PROTEIN KINASE KINASE 5 (MKK5), thereby interfering with signal transduction from activated pattern recognition receptors to the nucleus (Wang et al., 2010). HopF2 can also ADP-ribosylate Arabidopsis RIN4 *in vitro* (Wang et al., 2010). Over-expression of a HopF2 transgene in Arabidopsis prevents cleavage of RIN4 by the Cysteine protease T3E AvrRpt2 (Wilton et al., 2010). This indicates that HopF2 either ADP-ribosylates residues in the nitrate-induced (NOI) domains of RIN4 that are essential for processing by AvrRpt2, or that HopF2 binds to RIN4 and sterically prevents access to the sequences cleaved by AvrRpt2. RIN4 is targeted by additional T3Es from different *P. syringae* pathovars and it is guarded by the NLRs RESISTANCE TO P. SYRINGAE PV MACULICOLA 1 (RPM1) and RESISTANT TO P. SYRINGAE 2 (RPS2) against effector-induced manipulation in the Col-0 accession (Belkhadir et al., 2004). The T3E AvrRpm1 from *P. syringae* pv. *maculicola* ADP-ribosylates RIN4 proteins from Arabidopsis and soybean at two positions in their N- and C-terminal NOI domains (Redditt et al., 2019). In addition to RIN4, AvrRpm1 also modifies several sequence-related Arabidopsis NOI proteins by ADP-ribosylation (Redditt et al., 2019). Following identification of the ADP-ribosylation sites on soybean RIN4b by proteomics, Redditt et al. (2019) predicted, based on sequence homology, that AvrRpm1 modifies Arabidopsis RIN4 on N11 and D153. RPM1 is activated by modifications in the C-terminal NOI (C-NOI) of RIN4 (Chung et al., 2011) and a RIN4 D153A mutant variant that can no longer be ADP-ribosylated in the C-NOI attenuates AvrRpm1-induced activation of RPM1 (Redditt et al., 2019).

Previously, different approaches have been employed to identify substrates of plant-targeted bacterial ADP-ribosyltransferases. Fu et al. (2007) used ADP-ribosylation assays with ^{32}P-NAD^+ in plant cell extracts in combination with anion exchange chromatography and two-dimensional gel

electrophoresis to identify the RNA-binding protein GRP7 as a substrate of the T3E HopU1 from *Pst* DC3000. In other cases, prior knowledge about T3E interference with distinct immune signaling pathways and/or subcellular localization of bacterial ADP-ribosyltransferases in plant cells has aided in identification of potential host targets (Wang et al., 2010; Wilton et al., 2010; Zhou et al., 2014; Aung et al., 2020). For two plant substrates, ADPr modification sites have been determined by targeted *in vitro* ADP-ribosylation assays in combination with site-directed mutagenesis (Fu et al., 2007; Wang et al., 2010). Detection of ADP-ribosylation sites by proteomics following immunoprecipitation of presumed host target proteins from plant cell extracts has only recently been established and this approach so far relies on prior identification of effector targets and over-expression of epitope-tagged proteins (Redditt et al., 2019; Yoon et al., 2022). Given that putative host-targeted ADP-ribosyltransferases are not limited to *P. syringae* but also present in other bacterial and fungal plant pathogens (Seong and Krasileva, 2021) we sought to establish proteomics methods that can aid in direct detection of ADP-ribosylated proteins from plant protein extracts. Here we present a proteomics workflow that can identify ADP-ribosylated proteins from transgenic lines expressing a bacterial ADP-ribosyltransferase by comparative proteomics and provide site resolution for the ADP-ribosylated peptides.

Results

We used transgenic lines that express AvrRpm1-HA or HopF2-HA under control of a Dexamethasone (Dex)-inducible promoter to assess if ADP-ribosylated endogenous RIN4 protein (24 kDa) can be detected by immunoblot analysis. Samples from two independent AvrRpm1-expressing lines showed two bands between 25 and 35 kDa when probed with an antibody specific to mono-ADP-ribosylation (Bonfiglio et al., 2020). In contrast, the antibody did not detect prominent bands in the two lines expressing HopF2-HA (Fig. 1A). Even upon longer exposure, the band pattern of the HopF2 samples looked similar to those from Col-0 and two lines carrying a transgene encoding the enzymatically inactive HopF2 D175A variant. As shown by the anti-HA immunoblot in Fig. 1A, both HopF2-HA protein variants were expressed suggesting that HopF2 substrates might be proteins of low abundance or that they were not efficiently extracted from plant tissue by our method. Next, we used the engineered version of the Af1521 Macro domain (Nowak et al., 2020) to enrich ADP-ribosylated proteins from plant extracts (Fig. 1B). As the Af1521 Macro domain can also bind to the terminal ADPr of poly(ADPr) chains, the signal on the immunoblot probed with α-pan-ADPr binding reagent might represent a mixture of mono- and poly-ADP-ribosylated proteins. When analyzed by LC-MS/MS we identified 24 peptide spectra matches (PSM) of RIN4 in two samples from an AvrRpm1-expressing line but not in Col-0 or HopF2 samples (Table 1, Supplementary Dataset S1). However, this approach did not detect any ADP-ribosylated peptides of RIN4 or other proteins. We found that a depletion of potentially competing nucleotide analogs (Karras et al., 2005) by a Sephadex G-25 column resulted in stronger enrichment by the Af1521 Macro domain (Fig. 1C).

To further optimize detection of ADP-ribosylated peptides we focused on substrates of AvrRpm1. Untargeted proteomics of the pre-cleared and ADPr-enriched AvrRpm1 sample detected ADP-ribosylated peptides of the NOI sequences from NOI4 (AT5G55850.3), NOI12 (AT2G04410.1), as well as the N-NOI and C-NOI sequences of RIN4 (Supplementary Dataset S2). Although the marker ions of ADPr fragmentation (Ade^+ 136.06, AMP^+ 348.07, $ADPr^+$ 542.07 Da) and MaxQuant (Tyanova et al., 2016) Andromeda scores between 64 and 156 clearly identified these peptides as ADP-ribosylated (Fig. 1D), the localization probability for ADPr modification sites was often below 80% and therefore ambiguous. Next, we used a data-dependent acquisition (DDA) method that triggers an MS^2 scan with an elevated threshold for automatic gain control, higher resolution, and longer injection time upon detection of the 136.06 Da $Adenine^+$ fragment of ADPr that is typically an intense fragment ion from O-linked ADP-ribosylation sites (Rosenthal et al., 2015). The DDA method resulted in more informative ion series including additional neutral losses of AMP (Δ347.06 Da) (Fig. 2, Supplementary Dataset S3). Consequently, the ADPr localization probabilities improved to >80% and from three LC-MS/MS runs we could identify at least one MS^2 spectrum for each modified peptide with a localization score of >99.5%. Based on these data and the assumption that ADP-ribosylation does not occur on F, G, or W (Rack et al., 2020), the NOI4 protein was ADP-ribosylated on E29 (Fig. 2A) and for NOI12 we observed ADP-ribosylation on the sequence-equivalent position E13 (Fig. 2B). RIN4 was ADP-ribosylated on N11 (N-NOI, Fig. 2C) and D153 (C-NOI, Fig. 2D). ADP-ribosylation of these residues was further supported by manual inspection of MS^2 spectra exported from Proteome Discoverer that revealed presence of the respective b3* ions with a neutral loss of AMP (Supplementary Fig. S1). In conclusion, based on the AvrRpm1-RIN4 proof-of-concept experiments, our method robustly identified RIN4 and RIN4 homologs as *in planta* substrates of AvrRpm1 and allowed mapping the ADP-ribosylation sites with high confidence.

While MaxQuant reports several ADP-ribosylated peptides in addition to those from NOI4, NOI12, and RIN4, their MS^2 spectra overall had lower Andromeda scores and lacked the ADP-ribosylation marker ions that are typical for O-linked ADP-ribosylation (Supplementary Dataset S3). These spectra were also characterized by a higher signal to noise ratio and in many cases the incomplete b- and y-ion series did not cover the assumed ADP-ribosylation site. Therefore, the data did not provide sufficient evidence for ADP-ribosylation. One exception was a peptide from the MEMBRANE-ASSOCIATED MANNITOL-INDUCED (MAMI, AT5G54110.1) protein (Fig. 3A) that was identified in one of the three LC-MS/MS runs. In this case an almost complete y-ion series with neutral losses of AMP together with the Ade^+ and AMP^+ marker ions indicated ADP-ribosylation of peptide VVGEGLVIDEWKER (236-249) with the highest localization probabilities for E245 or K247 (underlined, 33% respectively). Manual inspection of the MS^2 spectrum revealed a better fit of the recorded spectrum to a peptide with ADPr on E245 (Supplementary Fig. S2). If MAMI is ADP-ribosylated by AvrRpm1, the protein should be enriched compared to controls in our ADPr affinity purification. Indeed, we identified MAMI with 27 PSM in ADPr-enriched samples of Dex-treated

AvrRpm1 plants but not in Dex-treated HopF2 or Col-0 controls (Table 1, Supplementary Dataset S1). Over-expression of AvrRpm1 may stabilize or elevate MAMI protein levels, which could result in higher carry-over of MAMI-derived peptides during the affinity enrichment. However, we consider this unlikely as we did not observe PSM for MAMI when we performed the enrichment with the Af1521 G42E variant (Dani et al., 2009) that does not bind ADPr (0 PSM G42E vs. 11 PSM Af1521; Table 1, Supplementary Dataset S4). We obtained further evidence for AvrRpm1-mediated ADP-ribosylation of MAMI from the transient *Nicotiana benthamiana* expression system. When AvrRpm1-Flag was co-expressed with a HA-tagged MAMI we observed an additional slower migrating band on the α-HA immunoblot (Fig. 3B). A band of ~37 kDa was also visible when the blot was probed with α-pan-ADPr (Fig. 3B), indicating that MAMI can be ADP-ribosylated by AvrRpm1. In LC-MS/MS analysis of samples from *N. benthamiana* leaves co-expressing AvrRpm1-Flag and HA-MAMI we detected the ADP-ribosylated MAMI peptide shown in Fig. 3A only in the pulldown with the functional Af1521 Macro domain but not the G42E control. Expression of HA-MAMI alone did not result in detectable ADP-ribosylation indicating that co-expression of AvrRpm1 was required for ADP-ribosylation of MAMI (Supplementary Dataset S5).

Apart from RIN4, NOIs, and MAMI several other proteins were enriched in ADPr pulldowns from AvrRpm1 plants in a G42-dependent manner and were not identified in Col-0 and HopF2 samples. This set includes PHOSPHOLIPASE D GAMMA 3 (PLDGAMMA3, AT4G11840.1) and the blue light photoreceptor PHOTOTROPIN 1 (PHOT1, AT3G45780.1) (Table 1; Supplementary Datasets S1, S4). Therefore, even if no ADP-ribosylated peptides can be identified, comparative pulldowns with the functional vs. non-functional Af1521 Macro domains can provide information on potentially modified proteins that can be further assessed for evidence of ADP-ribosylation by directed methods.

Discussion

In this study, we present a proteomics workflow that, regardless of prior knowledge, would have identified RIN4 and sequence-related NOI proteins as substrates of the host-targeted bacterial ADP-ribosyltransferase AvrRpm1 in Arabidopsis. Our data confirm the two ADP-ribosylation sites on the endogenous RIN4 protein that were predicted by Redditt et al. (2019) based on LC-MS/MS analysis of the soybean RIN4b protein. We further show that RIN4 homologs NOI4 and NOI12 are ADP-ribosylated at the sequence-equivalent site of the conserved NOI sequence indicating that AvrRpm1 preferentially modifies NOI proteins on Glu, Asp or Asn residues on the 5th position of the PKFG[E/D/N]W[E/D/N] consensus sequence. AvrRpm1 and the sequence-unrelated T3E AvrB indirectly promote RIN4 phosphorylation on T166 by receptor-like cytoplasmic kinases and it is the AvrRpm1-mediated manipulation of the RIN4 C-NOI sequence that is sensed by RPM1(Liu et al., 2011; Chung et al., 2011). Based on single and double mutant analysis of RIN4 D153 and T166, Redditt et al. (2019) hypothesized that ADP-ribosylation on D153 promotes phosphorylation of T166. In contrast, data from Yoon et al. (2022) indicate that AvrRpm1-mediated ADP-ribosylation of a RIN4

T166A mutant protein still triggers RPM1 activation. While we identified several previously reported RIN4 phosphorylation sites (S116, S141, and the peptide SSGANVSGSSRTPTHQSSR with phosphorylation on S186 or T188, Supplementary Dataset S6) (Willems et al., 2019), we did not detect phosphorylation on T166. However, given the relatively low abundance of ADP-ribosylated peptides from the RIN4 C-NOI, we consider this result inconclusive with respect to either of the two hypotheses for RPM1 activation. In the absence of NLR recognition, i. e. when AvrRpm1-expressing *P. syringae* bacteria are directly infiltrated into leaves of the *rpm1 rps2* double mutant, AvrRpm1 promotes bacterial virulence and this does not require RIN4 (Belkhadir et al., 2004). In this respect, plasma membrane-associated proteins like MAMI, PLDGAMMA3 or PHOT1 that are specifically ADPr-enriched from AvrRpm1-expressing plants might constitute potential virulence targets of AvrRpm1. Alternatively, modification of these proteins may represent off-target events resulting from over-expression of the Dex-induced AvrRpm1 effector.

In contrast to AvrRpm1, our approach did not identify substrates of HopF2. Multiple host targets of HopF2 have been proposed including MKK5, RIN4, and BAK1 (Wang et al., 2010; Wilton et al., 2010; Zhou et al., 2014). However, none of these proteins were enriched in ADPr affinity pulldowns from HopF2-expressing plant cell extracts (Supplementary Dataset S1). One possible explanation is that proteins targeted by HopF2 are of low abundance, not effectively extracted by our protein isolation method and/or rapidly degraded upon modification. However, at least for the proposed HopF2 target RIN4 we can exclude inappropriate extraction conditions or low abundance, as proven by the successful affinity enrichment of ADP-ribosylated RIN4 from transgenic lines expressing AvrRpm1. The Af1521 Macro domain has been used for proteome-wide profiling of ADP-ribosylation sites in mammalian cells and does not show strong preferences in terms of the modified amino acid (Martello et al., 2016; Hendriks et al., 2019). It remains possible that plant proteins ADP-ribosylated by HopF2 are further chemically modified in a way that prevents detection by α-ADPr antibodies and enrichment by the Af1521 Macro domain. Indeed, it has been suggested that HopF2 might not function as a canonical ADP-ribosyltransferase. Wilton et al. (2010) reported that incubation of HopF2 with purified RIN4 in presence of ^{32}P-NAD^{+} did not result in radio-labeling of RIN4. However, HopF2's contribution to bacterial virulence was dependent on the presumed catalytic residue D175 and RIN4 (Wilton et al., 2010). On the other hand, Wang et al. (2010) reported that HopF2 covalently modifies Arabidopsis MKK5 and RIN4 *in vitro* when incubated with biotin-17-NAD^{+}, ADPr, and ATP in a D175-dependent manner.

We envisage that the method presented here will facilitate untargeted proteomics approaches to identify substrates of ADP-ribosyltransferases in plants. LC-MS/MS profiling of proteins that are enriched by the Af1521 Macro domain but not the G42E mutant can provide information on plant proteins that are ADP-ribosylated by a particular effector by comparison to suitable controls. The DDA proteomics method has the potential to directly sequence modified ADPr-enriched peptides as

demonstrated for NOI4, NOI12, RIN4, and MAMI. Ideally, an efficient and specific enrichment by the Af1521 Macro domain, paired with detection of ADP-ribosylated peptides, will facilitate identification of plant proteins modified by host-targeted ADP-ribosyltransferases from pathogens.

Materials and Methods

Plant material, DNA constructs, bacterial strains, and growth conditions

The transgenic lines expressing Dex-inducible AvrRpm1-HA and HopF2-HA have been described (Mackey et al., 2002; Wilton et al., 2010). Arabidopsis plants were grown in controlled environment chambers with a 10 h light period and 22/18 °C day/night temperatures. To induce expression of T3Es, 4-week-old plants were sprayed with a solution containing 20 μM Dex and 0.01% Silwet-77 and leaves were harvested 16-18 h later. *N. benthamiana* seeds were sown on Flora clay (92% raised-bog peat, 0.15% salinity, pH 5-6), stratified for 3 days at 4°C, and then cultivated under long day (16 h light, 8 h dark) conditions at 22 °C and approximately 30% relative humidity in a greenhouse under supplementary light from Tungsten lamps at approximately 200 μmol s^{-1} m^{-2}. The G42E mutation in the engineered Af1521 Macro domain was introduced by site-directed mutagenesis in pGEX6P-1 (Nowak et al., 2020). The functional (K35E, Y145R) and non-functional (K35E, G42E, Y145R) variants were cloned into KpnI/HindIII-linearized pOPINF (Berrow et al., 2007) by Gibson cloning to create His6-GST-Macro constructs. The MAMI, PHOT1, and AvrRpm1 coding sequences as well as the genomic sequence of PLDGAMMA3 were cloned into pENTR4 by Gibson cloning. The N-terminally tagged StrepII-3xHA-MAMI construct was created by a Gateway LR reaction with pENS-HS-GW. The C-terminally tagged PHOT1-3xHA-StrepII and PLDGAMMA3-3xHA-StrepII constructs were created by Gateway LR reactions with pXCSG-GW-HS. AvrRpm1 was fused to a 3xFlag tag by a Gateway LR reaction with pTA7001/des/3XFlag (Li et al., 2013). Binary vectors were transformed into *Agrobacterium tumefaciens* strain GV3101 $pMP90^{RK}$ (pENS, pXCSG) or GV3101 pMP90 (pTA7001).

Agrobacterium-mediated transient expression

A. tumefaciens strains were grown on selective YEB plates and resuspended in infiltration buffer (10 mM $MgCl_2$, 10 mM MES-KOH pH 5.6, 150 μM acetosyringone). Each strain was mixed with *A. tumefaciens* strain GV3101 pMP90 expressing the silencing suppressor 19K at a ratio of 1:1. The cultures were infiltrated into leaves of 4-5 week-old *N. benthamiana* plants using a needleless syringe. After 2 days, AvrRpm1 expression was induced by spraying infiltrated leaves with Dex as above and leaf material for protein extraction was harvested 8 h later.

Plant protein extraction and detection by immunoblots

Protein extracts were prepared by grinding plant leaf material in liquid N_2 to a fine powder followed by resuspension in extraction buffer [50 mM Tris-HCl, 150 mM NaCl, 10% (v/v) glycerol, 1 mM EDTA, 5 mM DTT, 1× protease inhibitor cocktail (Sigma-Aldrich #P9599), 0.2% NP-40, pH 7.4] at a ratio of

2 mL buffer per 1 g leaf material. Crude protein extracts were centrifuged at 20000 x *g* / 4 °C / 20 min and the supernatant was either used for SDS-PAGE or subjected to ADPr-enrichment with the Af1521 Macro domain. For immunoblots, proteins were separated by SDS-PAGE and electro-blotted onto PVDF membrane. The membrane was blocked with 5% non-fat dry milk in TBST for 1 h at RT. Proteins were detected using α-HA 3F10 antibody (Merck, 11867423001, 1:4000), α-Flag M2 antibody (Merck, F3165, 1:1000), α-pan-ADPr binding reagent (Merck, MABE1016, 1:4000), or α-mono-ADPr AbD33204 (Bio-Rad, 1:2000) in 2.5% non-fat dry milk in TBST over night at 4 °C. Proteins were detected using HRP-coupled secondary antibodies.

Enrichment of ADP-ribosylated proteins

Per affinity purification 15 µL Glutathion-Sepharose 4B resin (Merck) was washed in 50 mM Tris-HCl pH 7.5, 50 mM NaCl, 1 mM DTT and pelleted by centrifugation (500 x *g*, RT, 1 min). 1, 2.5 or 5 µg of GST-Macro (or G42E) were added in a total volume of 1 mL wash buffer and the tubes were rotated for 1 h at 4 °C. The resin was pelleted as above and washed twice with 0.8 mL plant extraction buffer (see plant protein extraction section above) supplemented with 10 µM MG132 (Merck). Cold plant extract was either added directly to the resin (Supplementary Dataset S1) or pre-cleared by filtration over 1-3 stacked 5 mL HiTrap desalting columns (Cytiva) followed by collection of the protein fraction based on absorbance at 280 nm (Supplementary Datasets S2-S6). The samples were rotated for 2 h at 4 °C and washed three times with 1 mL cold plant extraction buffer. The proteins were eluted from the resin by adding SDS sample buffer and incubation at 75 °C for 5 min.

Protein expression and purification

The His6-GST-Macro variants were expressed in *E. coli* Shuffle cells (NEB). Cultures were grown in LB medium at a temperature of 37 °C to an OD_{600} of 1.0 – 1.2. The cultures were cooled to 18 °C before expression was induced by the addition of 0.5 mM IPTG for 16 h. Cells were pelleted by centrifugation (5000 x *g* / 4 °C / 12 min) and the pellets were resuspended in buffer A [50 mM Tris-HCl, 0.3 M NaCl, 20 mM imidazole, 5% (v/v) glycerol, 50 mM glycine, pH 8.0] supplemented with 0.1% polyethylenimine and 1x cOmplete™ EDTA-free protease inhibitor cocktail (Merck). Cells lysis was induced by addition of Lysozyme (1 mg/mL final concentration / 25 °C / 15 min) followed by sonication on ice (Branson 150D Sonifier, 2x 10 min, level 3-4). Insoluble proteins and cell debris were removed by centrifugation (30000 x *g* / 4 °C / 30 min) and the supernatant was loaded onto a 5 mL HisTrap HP IMAC column (Cytiva). The column was washed with buffer A until the A_{280} reached 25 mAU and proteins were eluted using buffer B [50 mM Tris-HCl, 0.3 M NaCl, 0.5 M imidazole, 5% (v/v) glycerol, 50 mM glycine, pH 8.0]. The elution from the IMAC column was injected onto a size exclusion chromatography column [Superdex 75 26/60 PG column (Cytiva) pre-equilibrated with 20 mM HEPES-NaOH, 150 mM NaC, pH 7.5]. Proteins eluting from the column were concentrated by ultrafiltration on Vivaspin 20 columns (Sartorius) with a 5 kDa molecular weight cut-off. The His6-tag was cleaved using 3C protease. The protein was run through a 5 mL HisTrap HP IMAC column in

buffer A to remove the His6-tag and residual un-cleaved fusion protein, followed by injection onto the Superdex 75 26/60 PG column and elution and concentration as above. Aliquots were snap-frozen in liquid N_2 and stored at -70 °C.

Sample preparation for LC-MS/MS

Protein samples were separated by 12% SDS-PAGE until the running front had migrated 1 cm into the separating gel. The gels were stained with Coomassie and the protein area was cut from the gel. Proteins were in-gel digested with trypsin and desalted as described by (Majovsky et al., 2014).

Acquisition of raw data sets by higher energy collisional dissociation (HCD) fragmentation

Peptides were analyzed with 5 different MS methods on a Fusion Lumos Tribrid mass spectrometer (Thermo Fisher Scientific), summarized in Supplementary Dataset S7. Dried peptides were dissolved in 5% acetonitrile, 0.1% trifluoric acid and injected into an EASY-nLC 1200 liquid chromatography system (Thermo Fisher Scientific). Peptides were separated using liquid chromatography C18 reverse phase chemistry employing a 120 min gradient increasing from 1 to 24 % acetonitrile in 0.1% FA (MS method 1) or from 1% to 36% acetonitrile in 0.1% FA (MS methods 2-5), and a flow rate of 250 nL/min. Eluted peptides were electrosprayed on-line into the Fusion Lumos Tribrid with a spray voltage of 2.0 kV and capillary temperature of 305°C. Peptides (MS^1) were detected in the Orbitrap with the following settings: resolving power: 120,000; scan range m/z 300–1500; S-Lens RF 30%; AGC target Standard, max injection time (IT) on Auto mode, microscans: 1. Dynamic exclusion duration was set for 60 s (MS method 1) or 30 s (MS methods 2-5). MS/MS peptide sequencing was performed using a Top15 DDA scan strategy (MS method 1), or peptides were selected for a 1 s time window in between master scans in a data-dependent mode (MS methods 2-5) with HCD at 30% NCE, to be detected in the Orbitrap with a resolution of 30000. For differences in AGC target and maximum injection time mode between different methods see Supplementary Dataset S7. Different targeted mass exclusion lists containing the most prominent peptide m/z ratios for the GST-Af1521 Macro domain and, where appropriate, GSTs from *A. thaliana* were used for MS methods 2, 3 and 5 (see Supplementary Dataset S7). For Methods 3-5, an additional MS^2 scan with an isolation window of 1.3 was triggered by the presence of the diagnostic peak of adenine at 136.062 Da in a precursor's fragmentation spectrum. Orbitrap detection occurred at a resolution of 60000 with a defined first mass of 120 m/z. The normalized AGC Target of the triggered scan was set to 1000% and the maximum injection time was 1800 ms.

Identification of proteins and peptides

For Supplementary Datasets S1 and S4, peptides and proteins were identified using the Mascot software v2.7.0 (Matrix Science) linked to Proteome Discoverer v2.4 (Thermo Fisher Scientific). The enzyme specificity was set to trypsin and two missed cleavages were tolerated. Carbamidomethylation of cysteine (C) was set as fixed modification, and oxidation of methionine (M)

as well as ADP-ribosylation of aspartic acid (D) or glutamic acid (E) or phosphorylation of serine (S) and threonine (T) as variable modifications. A precursor ion mass error of 10 ppm and a fragment ion mass error of 0.02 Da were tolerated in searches of the TAIR10 database amended with modified sequences of GST-Af1521 and common contaminants. A decoy database search was performed to determine the peptide spectral match (PSM) and peptide identification false discovery rates (FDR). Phosphorylated peptides with a score surpassing the false discovery rate threshold of 0.01 (q-value<0.01) were considered positive identifications. The phosphoRS module was used to specifically map ADP-ribosylation or phosphorylation to amino acid residues within the primary structure of peptides.

For Supplementary Datasets S2, S3, S5, and S6 peptides and proteins were identified using MaxQuant software v2.1.3.0 (Tyanova et al., 2016). For Supplementary Datasets S2, S3, and S6 the data were searched against the *A. thaliana* Araport11 proteome database downloaded from https://www.arabidopsis.org/download/ on 03.01.2022 and the sequences of the GST-Af1521 Macro domains. For Supplementary Datasets S5 peptides and proteins were identified by searches against the *N. benthamiana* NbDE proteome database (Kourelis et al., 2019) downloaded on 22.12.2022. The minimal peptide length was 7 amino acids, the enzyme specificity was set to Trypsin/P and two missed cleavages were tolerated. Carbamidomethylation of cysteine (C) was set as fixed modification. Variable modifications were oxidation of methionine (M), acetylated protein N-termini and ADP-ribosylation of aspartic acid (D), glutamic acid (E), asparagine (N), lysine (K), arginine (R), serine (S), cysteine (C), and histidine (H). Neutral losses of Adenine (135.0545 Da), AMP (347.0631 Da), Adenosine H_2O (249.0862 Da), ADP (427.0294 Da), and ADPr (541.0611 Da) were included for data analysis. Adenine$^+$ (136.0618 Da), AMP$^+$ (348.0704 Da), and ADPr$^+$ (542.0684 Da) were used as diagnostic peaks for ADP-ribosylation. For Supplementary Dataset S6 phosphorylation of serine (S) and threonine (T) was included as additional variable modification.

Availability of data and constructs

The following plasmids have been submitted to Addgene (https://www.addgene.org/): pENTR4-MAMI #209186, pENTR4-PHOT1 #209187, pENTR4-PLDGAMMA3 #209188, pENTR4-AvrRpm1 #209185. The pOPIN-F His6-GST-Af1521 Macro expression constructs are in part bound by a MTA with the University of Zurich and are, as all other materials, available upon request. The mass spectrometry proteomics data have been submitted to the ProteomeXchange Consortium via the PRIDE (Perez-Riverol et al., 2022) partner repository. Identifiers will be posted in the bioRxiv comments section.

Acknowledgements

We thank the following colleagues for sharing published materials: Jeff Dangl (Dex-AvrRpm1 lines in *rpm1-3* background), Darrell Desveaux (Dex-HopF2 lines), Michael Hottiger (pGEX-6p-1 Af1521 K35E/Y145R Macro domain), Gitta Coaker (pTA7001/des/3XFlag). LW acknowledges core funding

from the Leibniz Institute of Plant Biochemistry (IPB). We thank Jessica Erickson and Kee Hoon Sohn for helpful comments on the manuscript.

Author contributions

SK, TC, and LW conceived and designed experiments. SK, DT, CP, and LW carried out experiments. SK, TC, SM, IM, and LW analyzed the data. LW wrote the manuscript with input from all co-authors. All authors reviewed and approved the submitted manuscript.

References

Aung, K., Kim, P., Li, Z., Joe, A., Kvitko, B., Alfano, J.R., and He, S.Y. (2020). Pathogenic Bacteria Target Plant Plasmodesmata to Colonize and Invade Surrounding Tissues. Plant Cell **32**: 595–611.

Belkhadir, Y., Nimchuk, Z., Hubert, D.A., Mackey, D., and Dangl, J.L. (2004). Arabidopsis RIN4 negatively regulates disease resistance mediated by RPS2 and RPM1 downstream or independent of the NDR1 signal modulator and is not required for the virulence functions of bacterial type III effectors AvrRpt2 or AvrRpm1. Plant Cell **16**: 2822–2835.

Berrow, N.S., Alderton, D., Sainsbury, S., Nettleship, J., Assenberg, R., Rahman, N., Stuart, D.I., and Owens, R.J. (2007). A versatile ligation-independent cloning method suitable for high-throughput expression screening applications. Nucleic Acids Res. **35**: e45.

Bonfiglio, J.J., Leidecker, O., Dauben, H., Longarini, E.J., Colby, T., San Segundo-Acosta, P., Perez, K.A., and Matic, I. (2020). An HPF1/PARP1-Based Chemical Biology Strategy for Exploring ADP-Ribosylation. Cell **183**: 1086–1102.

Chung, E.-H., da Cunha, L., Wu, A.-J., Gao, Z., Cherkis, K., Afzal, A.J., Mackey, D., and Dangl, J.L. (2011). Specific threonine phosphorylation of a host target by two unrelated type III effectors activates a host innate immune receptor in plants. Cell Host Microbe **9**: 125–136.

Cunnac, S., Chakravarthy, S., Kvitko, B.H., Russell, A.B., Martin, G.B., and Collmer, A. (2011). Genetic disassembly and combinatorial reassembly identify a minimal functional repertoire of type III effectors in *Pseudomonas syringae*. Proc. Natl. Acad. Sci. U.S.A. **108**: 2975–2980.

Dani, N., Stilla, A., Marchegiani, A., Tamburro, A., Till, S., Ladurner, A.G., Corda, D., and Di Girolamo, M. (2009). Combining affinity purification by ADP-ribose-binding macro domains with mass spectrometry to define the mammalian ADP-ribosyl proteome. Proc Natl Acad Sci U S A **106**: 4243–4248.

Fu, Z.Q., Guo, M., Jeong, B., Tian, F., Elthon, T.E., Cerny, R.L., Staiger, D., and Alfano, J.R. (2007). A type III effector ADP-ribosylates RNA-binding proteins and quells plant immunity. Nature **447**: 284–288.

Hendriks, I.A., Larsen, S.C., and Nielsen, M.L. (2019). An Advanced Strategy for Comprehensive Profiling of ADP-ribosylation Sites Using Mass Spectrometry-based Proteomics. Mol Cell Proteomics **18**: 1010–1026.

Karras, G.I., Kustatscher, G., Buhecha, H.R., Allen, M.D., Pugieux, C., Sait, F., Bycroft, M., and Ladurner, A.G. (2005). The macro domain is an ADP-ribose binding module. EMBO J **24**: 1911–1920.

Kourelis, J., Kaschani, F., Grosse-Holz, F.M., Homma, F., Kaiser, M., and van der Hoorn, R.A.L. (2019). A homology-guided, genome-based proteome for improved proteomics in the alloploid *Nicotiana benthamiana*. BMC Genomics **20**: 722.

Li, W., Chiang, Y.-H., and Coaker, G. (2013). The HopQ1 Effector's Nucleoside Hydrolase-Like Domain Is Required for Bacterial Virulence in Arabidopsis and Tomato, but Not Host Recognition in Tobacco. PLoS One **8**: e59684.

Liu, J., Elmore, J.M., Lin, Z.-J.D., and Coaker, G. (2011). A receptor-like cytoplasmic kinase phosphorylates the host target RIN4, leading to the activation of a plant innate immune receptor. Cell Host Microbe **9**: 137–146.

Mackey, D., Holt, B.F., Wiig, A., and Dangl, J.L. (2002). RIN4 interacts with *Pseudomonas syringae* type III effector molecules and is required for RPM1-mediated resistance in Arabidopsis. Cell **108**: 743–754.

Majovsky, P., Naumann, C., Lee, C.-W., Lassowskat, I., Trujillo, M., Dissmeyer, N., and Hoehenwarter, W. (2014). Targeted proteomics analysis of protein degradation in plant signaling on an LTQ-Orbitrap mass spectrometer. J Proteome Res **13**: 4246–4258.

Martello, R., Leutert, M., Jungmichel, S., Bilan, V., Larsen, S.C., Young, C., Hottiger, M.O., and Nielsen, M.L. (2016). Proteome-wide identification of the endogenous ADP-ribosylome of mammalian cells and tissue. Nat Commun **7**: 12917.

Martin, R., Qi, T., Zhang, H., Liu, F., King, M., Toth, C., Nogales, E., and Staskawicz, B.J. (2020). Structure of the activated ROQ1 resistosome directly recognizing the pathogen effector XopQ. Science **370**: eabd9993.

Neuhauser, N., Michalski, A., Cox, J., and Mann, M. (2012). Expert system for computer-assisted annotation of MS/MS spectra. Mol Cell Proteomics **11**: 1500–1509.

Nowak, K., Rosenthal, F., Karlberg, T., Bütepage, M., Thorsell, A.-G., Dreier, B., Grossmann, J., Sobek, J., Imhof, R., Lüscher, B., Schüler, H., Plückthun, A., Leslie Pedrioli, D.M., and Hottiger, M.O. (2020). Engineering Af1521 improves ADP-ribose binding and identification of ADP-ribosylated proteins. Nat Commun **11**: 5199.

Perez-Riverol, Y., Bai, J., Bandla, C., García-Seisdedos, D., Hewapathirana, S., Kamatchinathan, S., Kundu, D.J., Prakash, A., Frericks-Zipper, A., Eisenacher, M., Walzer, M., Wang, S., Brazma, A., and Vizcaíno, J.A. (2022). The PRIDE database resources in 2022: a hub for mass spectrometry-based proteomics evidences. Nucleic Acids Res **50**: D543–D552.

Rack, J.G.M., Palazzo, L., and Ahel, I. (2020). (ADP-ribosyl)hydrolases: structure, function, and biology. Genes Dev **34**: 263–284.

Redditt, T.J., Chung, E.-H., Karimi, H.Z., Rodibaugh, N., Zhang, Y., Trinidad, J.C., Kim, J.H., Zhou, Q., Shen, M., Dangl, J.L., Mackey, D., and Innes, R.W. (2019). AvrRpm1 Functions as an ADP-Ribosyl Transferase to Modify NOI Domain-Containing Proteins, Including Arabidopsis and Soybean RPM1-Interacting Protein4. Plant Cell **31**: 2664–2681.

Rosenthal, F., Nanni, P., Barkow-Oesterreicher, S., and Hottiger, M.O. (2015). Optimization of LTQ-Orbitrap Mass Spectrometer Parameters for the Identification of ADP-Ribosylation Sites. J Proteome Res **14**: 4072–4079.

Saur, I.M.L., Panstruga, R., and Schulze-Lefert, P. (2021). NOD-like receptor-mediated plant immunity: from structure to cell death. Nat Rev Immunol **21**: 305–318.

Seong, K. and Krasileva, K.V. (2021). Computational Structural Genomics Unravels Common Folds and Novel Families in the Secretome of Fungal Phytopathogen *Magnaporthe oryzae*. Mol Plant Microbe Interact **34**: 1267–1280.

Tyanova, S., Temu, T., and Cox, J. (2016). The MaxQuant computational platform for mass spectrometry-based shotgun proteomics. Nat Protoc **11**: 2301–2319.

Wang, J., Hu, M., Wang, J., Qi, J., Han, Z., Wang, G., Qi, Y., Wang, H.-W., Zhou, J.-M., and Chai, J. (2019). Reconstitution and structure of a plant NLR resistosome conferring immunity. Science **364**: eaav5870.

Wang, Y., Li, J., Hou, S., Wang, X., Li, Y., Ren, D., Chen, S., Tang, X., and Zhou, J.-M. (2010). A *Pseudomonas syringae* ADP-ribosyltransferase inhibits Arabidopsis mitogen-activated protein kinase kinases. Plant Cell **22**: 2033–2044.

Wang, Y., Pruitt, R.N., Nürnberger, T., and Wang, Y. (2022). Evasion of plant immunity by microbial pathogens. Nat Rev Microbiol **20**: 449–464.

Willems, P., Horne, A., Van Parys, T., Goormachtig, S., De Smet, I., Botzki, A., Van Breusegem, F., and Gevaert, K. (2019). The Plant PTM Viewer, a central resource for exploring plant protein modifications. Plant J. **99**: 752–762.

Wilton, M., Subramaniam, R., Elmore, J., Felsensteiner, C., Coaker, G., and Desveaux, D. (2010). The type III effector HopF2Pto targets Arabidopsis RIN4 protein to promote *Pseudomonas syringae* virulence. Proc. Natl. Acad. Sci. U.S.A. **107**: 2349–2354.

Xin, X.-F., Nomura, K., Aung, K., Velásquez, A.C., Yao, J., Boutrot, F., Chang, J.H., Zipfel, C., and He, S.Y. (2016). Bacteria establish an aqueous living space in plants crucial for virulence. Nature **539**: 524–529.

Yoon, M., Middleditch, M.J., and Rikkerink, E.H.A. (2022). A conserved glutamate residue in RPM1-INTERACTING PROTEIN4 is ADP-ribosylated by the Pseudomonas effector AvrRpm2 to activate RPM1-mediated plant resistance. Plant Cell **34**: 4950–4972.

Zhou, J., Wu, S., Chen, X., Liu, C., Sheen, J., Shan, L., and He, P. (2014). The *Pseudomonas syringae* effector HopF2 suppresses Arabidopsis immunity by targeting BAK1. Plant J **77**: 235–245.

Figure legends

Figure 1. ADP-ribosylated substrates of AvrRpm1 but not HopF2 can be detected by immunoblots, enriched by the engineered Af1521 Macro domain, and identified by untargeted proteomics from transgenic lines expressing the respective type III effectors. **(A)** Detection of AvrRpm1 substrates by an α-ADPr immunoblot. Protein extracts from Dex-treated Col-0 wild type and the indicated transgenic lines were separated by SDS-PAGE, electroblotted onto PVDF membrane and probed with α-HA and α-mono-ADPr antibodies. CBB = Coomassie Brilliant Blue-stained membrane as loading control. **(B)** Enrichment of ADP-ribosylated proteins from the indicated Arabidopsis lines by the engineered Af1521 Macro domain and detection in an α-pan-ADPr immunoblot. Approximately 15% of the ADPr-enriched fraction was loaded onto the gel. 'sol. extract' = soluble protein extract. The membrane was stained with Amido Black as loading control. This experiment was repeated once with similar results. **(C)** Depletion of potentially competing nucleotide analogs from plant

extracts prior to the Af1521 affinity purification facilitates enrichment of ADP-ribosylated proteins. 'Col-0' and 'AvrRpm1-HA #18' indicate the respective protein extracts before ADPr-enrichment. 'ADPr-enriched' = AvrRpm1 sample, direct pulldown with the Af1521 Macro domain. 'G-25->ADPr-enriched' = AvrRpm1 sample, pre-clearing by G-25 sepharose followed by pulldown with the Af1521 Macro domain. ADP-ribosylated proteins were detected as in (B). **(D)** HCD MS^2 spectrum of the ADP-ribosylated peptide FGDWDENNPSSADGYTHIFNK from the RIN4 C-NOI identified by untargeted proteomics (z = 3, mass = 2954.09 Da). Unmodified fragment ions and fragment ions with a neutral loss of AMP are indicated in the sequence logos. The horizontal line designates the possible sequence window for ADP-ribosylation. The ADPr marker ions are shown in beige. Asterisks indicate b-ions with a neutral loss of AMP (Δ347.06 Da).

Figure 2. ADPr-modification sites on AvrRpm1 substrates revealed by data-dependent HCD fragmentation. Panels A-D show MS^2 spectra of ADP-ribosylated peptides from NOI4, NOI12, and the RIN4 N-NOI and C-NOI sequences. Unmodified fragment ions and fragment ions with a neutral loss of AMP are indicated in the sequence logos. The horizontal line designates the possible sequence window for ADP-ribosylation. **(A)** NOI4-derived peptide FGEWDVNDPASAEGFTVIFNK (z = 3, mass = 2883.17 Da). **(B)** NOI12-derived peptide FGEWDVNDPSSAEGFTVIFNK (z = 3, mass = 2899.14 Da). **(C)** RIN4 N-NOI-derived peptide FGNWEAEENVPYTAYFDK (z = 3, mass = 2720.01 Da). **(D)** RIN4 C-NOI-derived peptide FGDWDENNPSSADGYTHIFNK (z = 3, mass = 2954.09 Da). The ADPr marker ions are shown in beige. Asterisks indicate ions with a neutral loss of AMP (Δ347.06 Da).

Figure 3. AvrRpm1 ADP-ribosylates Arabidopsis MAMI. **(A)** HCD MS^2 spectrum of the ADP-ribosylated MAMI peptide VVGEGLVIDEWKER (z = 3, mass = 2168.92 Da). The ADPr marker ions are shown in beige. Unmodified y-ions and y-ions with a neutral loss of AMP are indicated above the sequence logo. The horizontal line designates the possible sequence window for ADP-ribosylation. Asterisks indicate ions with a neutral loss of AMP (Δ347.06 Da). **(B)** Detection of ADP-ribosylated StrepII-3xHA-MAMI transiently co-expressed with AvrRpm1-3xFlag in *N. benthamiana*. Protein extracts were separated by SDS-PAGE, electroblotted onto PVDF membrane and probed with α-HA, α-pan-ADPr, or α-Flag antibodies. The membrane was stained with Amido Black as loading control. This experiment was repeated once with similar results. '19K' indicates a sample from leaves expressing only the silencing suppressor 19K.

Supplementary Figure S1. Analysis of MS^2 spectra from the ADP-ribosylated NOI4, NOI12, and RIN4 peptides supports ADP-ribosylation on position 3 of the FGxW motif. Peak lists of the MS^2 spectra shown in Fig. 2A-D were exported from Proteome Discoverer software and imported into the Expert system for computer-assisted annotation of MS/MS spectra (Neuhauser et al., 2012). Presence of the respective b3* ions with a neutral loss of AMP indicates ADP-ribosylation on E29 (NOI4, panel

A), E13 (NOI12, panel **B**), N11 (RIN4 N-NOI, panel **C**), and D153 (RIN4 C-NOI, panel **D**) as F and G are unlikely to be ADP-ribosylated.

Supplementary Figure S2. Analysis of the MS^2 spectrum from the ADP-ribosylated MAMI peptide. The peak list of the MS^2 spectrum shown in Fig. 3A was exported from Proteome Discoverer software and imported into the Expert system for computer-assisted annotation of MS/MS spectra (Neuhauser et al., 2012). **(A)** Match of the AMP neutral loss series assuming ADP-ribosylation on E245. The unmodified y2 and y3 ions are present. **(B)** Match of the AMP neutral loss series assuming ADP-ribosylation on E248. y2 and y3 ions with a neutral loss of AMP were not detected and ADPr on E248 does not allow annotation of additional peaks as compared to the model in (A).

Supplementary Dataset S1. Proteins identified by untargeted proteomics in two Af1521 Macro pulldown experiments from Dex-treated Col-0, AvrRpm1-HA, and HopF2-HA plants.

Supplementary Dataset S2. ADP-ribosylated peptides identified in three Af1521 Macro pulldown experiments from AvrRpm1-HA samples. For ADPr-enrichment, either 1, 2.5 or 5 μg of the engineered Af1521 Macro domain was added to the protein extract. The data was analyzed with MaxQuant and the output file 'ADP-ribosylationSites.txt' and the information on the corresponding MS^2 spectra from file 'msms.txt' were combined into one .xls file.

Supplementary Dataset S3. ADP-ribosylated peptides identified in three Af1521 Macro pulldown experiments from AvrRpm1-HA samples by the DDA method. For ADPr-enrichment, either 1, 2.5 or 5 μg of the engineered Af1521 Macro domain was added to the protein extract. The data was analyzed with MaxQuant and the output file 'ADP-ribosylationSites.txt' and the information on the corresponding MS^2 spectra from file 'msms.txt' were combined into one .xls file.

Supplementary Dataset S4. Comparison of proteins identified using the functional (Af1521) versus non-functional (G42E) Macro domains following ADPr-enrichment of proteins from Dex-treated AvrRpm1-HA plants.

Supplementary Dataset S5. *N. benthamiana* tissue expressing either AvrRpm1-3xFlag, StrepII-3xHA-MAMI, or co-expressing AvrRpm1-3xFlag and StrepII-3xHA-MAMI were subjected to ADPr-enrichment by the functional (Af1521) versus non-functional (G42E) Macro domains. The data was analyzed with MaxQuant and the output files 'evidence.txt', 'ADP-ribosylationSites.txt' and the information on the corresponding MS^2 spectra from file 'msms.txt' were combined into one .xls file.

Supplementary Dataset S6. The data from Supplementary Dataset S3 were analyzed for phosphorylation on S and T and ADP-ribosylation using MaxQuant. The output files 'Phospho

(ST)Sites.txt', 'ADP-ribosylationSites.txt' and the information on the corresponding MS^2 spectra from file 'msms.txt' were combined into one .xls file.

Supplementary Dataset S7. Detailed description of proteomics methods used in this work.

Table 1. Proteins specifically identified in Af1521 Macro-enriched AvrRpm1-HA samples (≥ 10 PSM) are not or not strongly enriched by the Af1521 G42E mutant variant.

AGI identifier	**description**	**PSM Col-0**	**PSM AvrRpm1**	**PSM HopF2**	**PSM ratio Af1521 / G42E**
AT4G11840.1	PLDGAMMA3	0	35	0	28 / 0
AT3G45780.1	PHOT1	0	29	0	27 / 0
AT5G54110.1	MAMI	0	27	0	11 / 0
AT3G25070.1	RIN4	0	24	0	27 / 6
AT3G24550.1	PERK1	0	18	0	5 / 0
AT1G70940.1	PIN3	0	14	0	0 / 0
AT5G39590.1	TLD-domain containing nucleolar protein	0	12	0	6 / 0
AT1G30470.1	SIT4 phosphatase-associated family protein	0	11	0	4 / 0
AT5G53000.1	TAP46	0	10	0	22 / 4

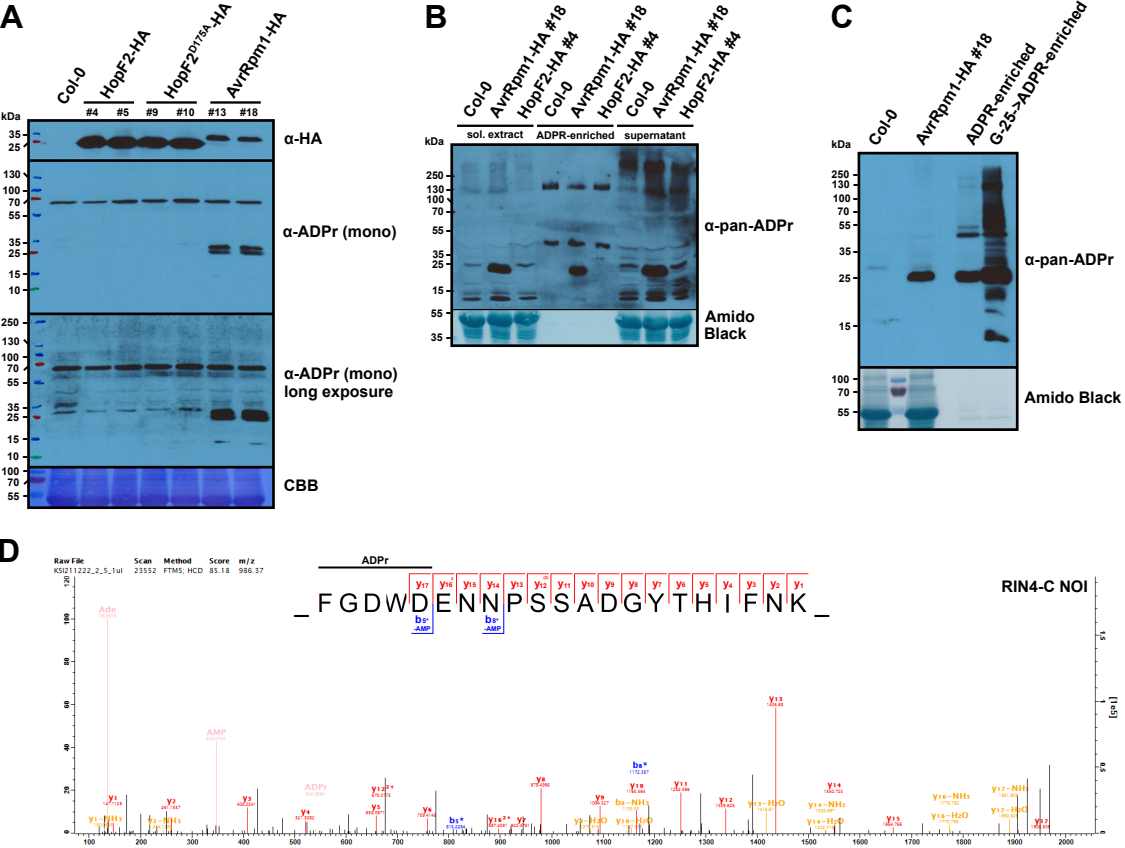

Figure 1. ADP-ribosylated substrates of AvrRpm1 but not HopF2 can be detected by immunoblots, enriched by the engineered Af1521 Macro domain, and identified by untargeted proteomics from transgenic lines expressing the respective type III effectors. **(A)** Detection of AvrRpm1 substrates by an α-ADPr immunoblot. Protein extracts from Dex-treated Col-0 wild type and the indicated transgenic lines were separated by SDS-PAGE, electroblotted onto PVDF membrane and probed with α-HA and α-mono-ADPr antibodies. CBB = Coomassie Brilliant Blue-stained membrane as loading control. **(B)** Enrichment of ADP-ribosylated proteins from the indicated Arabidopsis lines by the engineered Af1521 Macro domain and detection in an α-pan-ADPr immunoblot. Approximately 15% of the ADPr-enriched fraction was loaded onto the gel. 'sol. extract' = soluble protein extract. The membrane was stained with Amido Black as loading control. This experiment was repeated once with similar results. **(C)** Depletion of potentially competing nucleotide analogs from plant extracts prior to the Af1521 affinity purification facilitates enrichment of ADP-ribosylated proteins. 'Col-0' and 'AvrRpm1-HA #18' indicate the respective protein extracts before ADPr-enrichment. 'ADPr-enriched' = AvrRpm1 sample, direct pulldown with the Af1521 Macro domain. 'G-25->ADPr-enriched' = AvrRpm1 sample, pre-clearing by G-25 sepharose followed by pulldown with the Af1521 Macro domain. ADP-ribosylated proteins were detected as in (B). **(D)** HCD MS^2 spectrum of the ADP-ribosylated peptide FGDWDENNPSSADGYTHIFNK from the RIN4 C-NOI identified by untargeted proteomics (z = 3, mass = 2954.09 Da). Unmodified fragment ions and fragment ions with a neutral loss of AMP are indicated in the sequence logos. The horizontal line designates the possible sequence window for ADP-ribosylation. The ADPr marker ions are shown in beige. Asterisks indicate b-ions with a neutral loss of AMP (Δ347.06 Da).

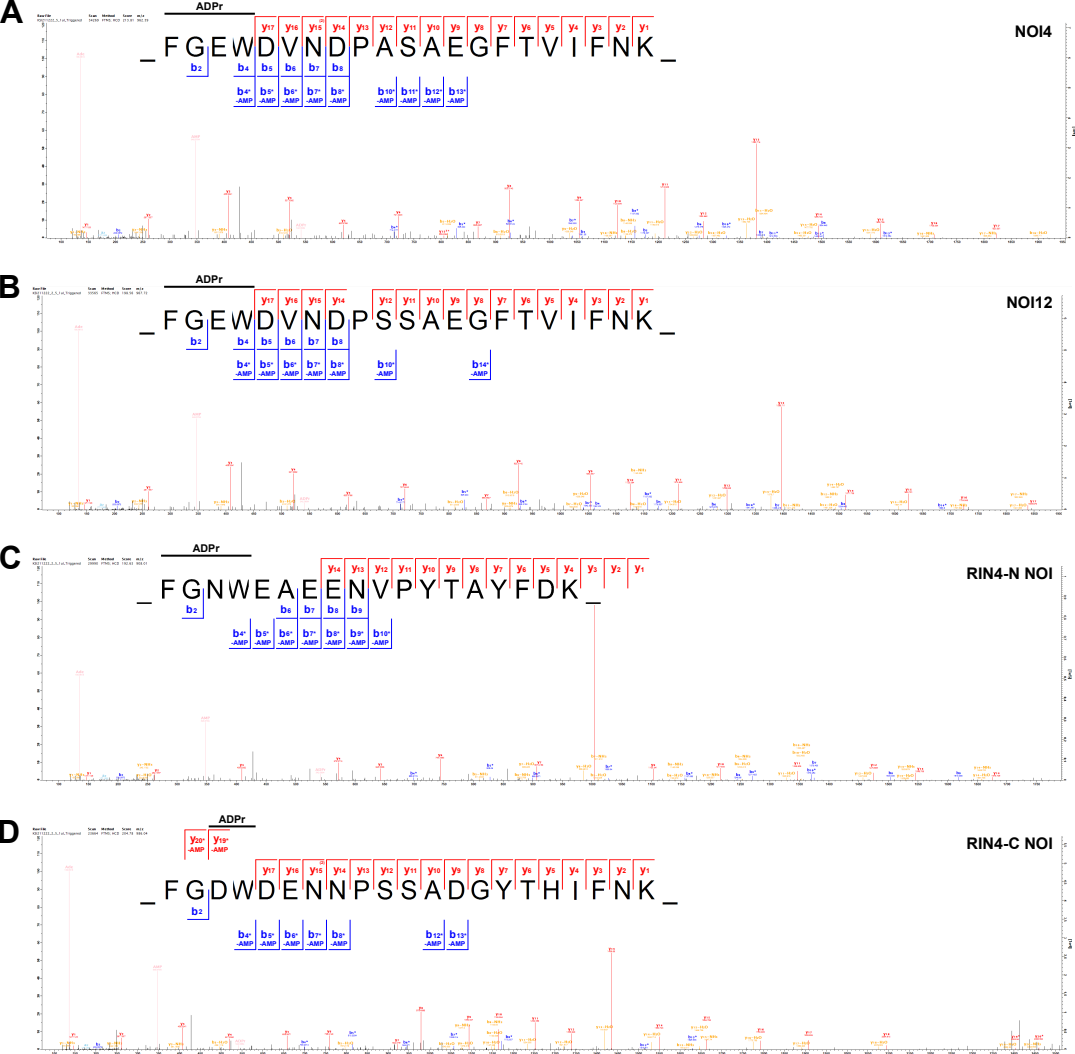

Figure 2. ADPr-modification sites on AvrRpm1 substrates revealed by data-dependent HCD fragmentation. Panels A-D show MS^2 spectra of ADP-ribosylated peptides from NOI4, NOI12, and the RIN4 N-NOI and C-NOI sequences. Unmodified fragment ions and fragment ions with a neutral loss of AMP are indicated in the sequence logos. The horizontal line designates the possible sequence window for ADP-ribosylation. **(A)** NOI4-derived peptide FGEWDVNDPASAEGFTVIFNK (z = 3, mass = 2883.17 Da). **(B)** NOI12-derived peptide FGEWDVNDPSSAEGFTVIFNK (z = 3, mass = 2899.14 Da). **(C)** RIN4 N-NOI-derived peptide FGNWEAEENVPYTAYFDK (z = 3, mass = 2720.01 Da). **(D)** RIN4 C-NOI-derived peptide FGDWDENNPSSADGYTHIFNK (z = 3, mass = 2954.09 Da). The ADPr marker ions are shown in beige. Asterisks indicate ions with a neutral loss of AMP (Δ347.06 Da).

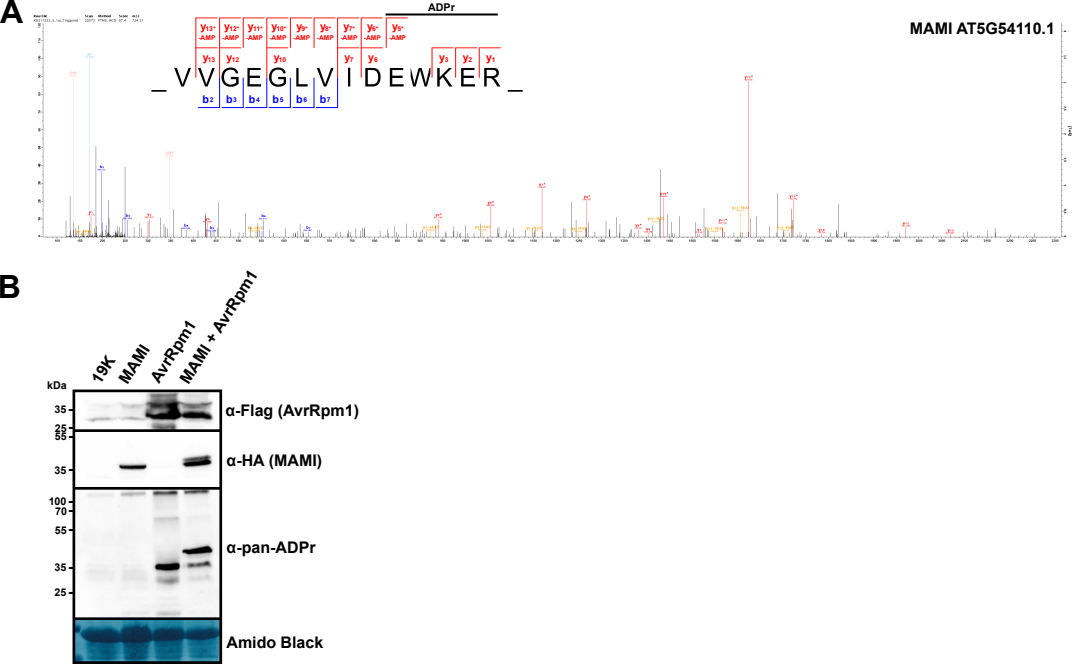

Figure 3. AvrRpm1 ADP-ribosylates Arabidopsis MAMI. **(A)** HCD MS^2 spectrum of the ADP-ribosylated MAMI peptide VVGEGLVIDEWKER (z = 3, mass = 2168.92 Da). The ADPr marker ions are shown in beige. Unmodified y-ions and y-ions with a neutral loss of AMP are indicated above the sequence logo. The horizontal line designates the possible sequence window for ADP-ribosylation. Asterisks indicate ions with a neutral loss of AMP (Δ347.06 Da). **(B)** Detection of ADP-ribosylated StrepII-3xHA-MAMI transiently co-expressed with AvrRpm1-3xFlag in *N. benthamiana*. Protein extracts were separated by SDS-PAGE, electroblotted onto PVDF membrane and probed with α-HA, α-pan-ADPr, or α-Flag antibodies. The membrane was stained with Amido Black as loading control. This experiment was repeated once with similar results. '19K' indicates a sample from leaves expressing only the silencing suppressor 19K.